Electronic Supplementary Material (ESI) for Environmental Science: Nano.

Supplementary data

for

Sedimentation kinetics and stability mechanisms of iron and manganese colloids in simulated groundwater solution

Shuxin Huang[a], Caixiang, Zhang[a,b]*, Lu Chen[a], Ruihan Xiong[a], Jiasen Li[a], Jidao Xie[a], Zenghui Fan[a], You Lv[a]

[a] State Key Laboratory of Biogeology and Environmental Geology, China University of Geosciences, Wuhan, 430078, China

[b] Hubei Key Laboratory of Yangtze Catchment Environmental Aquatic Science, Wuhan 430074, China

Corresponding author

E-mail address: cxzhang@cug.edu.cn (Prof. Caixiang Zhang).

Tel: +86 13971579235

Fax: +86 27 67883456

Summary

16 Pages, 8 Figures, 2 Tables

SUPPLEMENTAL MATERIALS AND METHODS

S1: Iron and manganese minerals Synthesis.

Goethite were synthesized by using the method of Paterson[1] and Wang et al.[2]. Briefly, 180 mL of 5 M NaOH was titrated to 100 mL of 1 M $FeCl_3 \cdot 6H_2O$ while stirring. The mixture was immediately diluted with deionized water and held in electric thermostatic drying oven at 60°C for 60 h. Ferrihydrite was synthesized by titrating dissolved $Fe(NO_3) \cdot 9H_2O$ with 330 mL of 1 M KOH[3]. The mixture pH was adjusted about 7-8. The main component of pyrolusite is manganese dioxide, and its synthesis were described by Perez-Benito et al.[4]. In brief, 20 mL of 1.9 M sodium thiosulfate was added to100 mL of 1.0 M potassium permanganate solution, and the mixture was diluted to 2 L. Birnessite was synthesized according to the method described by Tong et al.[5]. In brief, 170 mL of hydrochloric acid was added to 2.5 L of 1.0 M boiling potassium permanganate solution, and then the precipitate was rinsed with deionized water until the pH of the supernatant was about 4. All the synthesized minerals were purified through 10 cycles of deionized water washes, ground with ball mill, and passed through a 200-mesh standard nylon sieve, freeze-dried, and then stored in glass desiccator before use.

S2: DLVO theory.

The main interactions acting on Gt_C, Fh_C, Md_C, and Br_C under different electrolytes include the attractive energy (V_A, e.g. van der Waals energy) and the repulsive energy (V_R, e.g. electric double layer energy), described by the DLVO model[6, 7]. Therefore, the total interaction energy (V_T) could be calculated using the Eq. (1)[8], where V_A is given in Eq. (2)[9], and V_R is computed by the linear super position approximation expression, given in Eq. (3)[10].

$$V_T = V_A + V_R \quad (1)$$

$$V_A = -\frac{Ar}{12h\left(1 + \frac{14h}{\lambda}\right)} \quad (2)$$

$$V_R = 32\pi\varepsilon_0\varepsilon_r r\left(\frac{k_B T}{ze}\right)^2 \Gamma^2 exp(-\kappa h) \quad (3)$$

where A is the Hamaker constant, r is the particle radius, h is the distance between the surfaces of particles, λ is the characteristic wavelength of the dielectric (assumed to be 100 nm), ε_0 is the vacuum dielectric permittivity, 8.9 × 10^{-12} F/m, ε_r is the relative dielectric permittivity of water, equal to 78.5, T is the temperature, K, k_B is the Boltzmann constant, 1.4 × 10^{-23} J/K, z is the charge of the background ions, e is the electron charge, 1.6 × 10^{-19} C, Γ is the dimensionless surface potential for particles according to Eq. (4), κ is the reciprocal of the Debye length, given by Eq. (5)[11].

$$\Gamma = \tanh\left(\frac{ze\psi}{4k_B T}\right) \quad (4)$$

$$\kappa = \left(\frac{2e^2 N_A I}{\varepsilon_0\varepsilon_r k_B T}\right)^{1/2} \quad (5)$$

where ψ is the surface potential, N_A is Avogadro's constant, 6.0 × 10^{23}, I is ionic strength.

In the DLVO theory calculation, the surface potential of each colloid was considered equal to the zeta potential value. In addition, the Hamaker constant values of Gt_C, Fh_C, Md_C, and Br_C are 5.5 × 10^{-20}, 5.0 × 10^{-20}, 7.8 × 10^{-20}, and 6.6 × 10^{-20} J, respectively[11-13]. The radius of Gt_C, Fh_C, Md_C, and Br_C was calculated according to the DLS results.

When the background electrolyte concentration approached the critical coagulation concentration (CCC), the repulsive energy (V_R) was less than or equal to the attractive energy (V_A). The CCC can be determined theoretically by Eq. 6[14].

$$C_{CCC} = 1.51 \times 10^{80} \frac{(\varepsilon_0\varepsilon_r)^3 (k_B T)^5 \Gamma^4}{N_A e^2 A^2} \frac{1}{Z^6} \quad (6)$$

S3: XDLVO theory.

To better understand effect of the FA on colloidal stability, the total steric interaction energy (including a repulsive osmotic energy, V_{osm}, and an elastic repulsive energy, V_{elas}) between a polymer coated colloid

and an uncoated collector surface was introduced by the XDLVO theory. The expressions for V_{osm} and V_{elas} was given by Eq. 7-11[11].

$$\frac{V_{osm}}{k_BT} = \frac{4\pi r}{v_1}\varphi_p^2\left(\frac{1}{2}-\chi\right)l^2\left(\frac{h}{2l}-\frac{1}{4}-ln\left(\frac{h}{l}\right)\right) \quad h<l \quad (7)$$

$$\frac{V_{osm}}{k_BT} = \frac{2\pi r}{v_1}\varphi_p^2\left(\frac{1}{2}-\chi\right)\left(l-\frac{h}{2}\right)^2 \quad l\leq h\leq 2l \quad (8)$$

$$\frac{V_{osm}}{k_BT} = 0 \quad h>2l \quad (9)$$

$$\frac{V_{elas}}{k_BT} = \frac{2\pi r}{M_W}\varphi_P l^2\rho_P\left[\frac{h}{l}ln\left(\frac{h}{l}\left(\frac{3-\frac{h}{l}}{2}\right)^2\right)-6ln\left(\frac{3-\frac{h}{l}}{2}\right)+3\left(1-\frac{h}{l}\right)^2\right] \quad h<l \quad (10)$$

$$\frac{V_{elas}}{k_BT} = 0 \quad h\geq l \quad (11)$$

Where v_1 is the volume of a solvent molecule, equal to 0.03 nm^3; χ is the Flory-Huggins solvency parameter, which was assumed to be 0.45; l is the thickness of adsorbed FA (2.25 nm for Gt_C, 192.8 nm for Fh_C, and 30.2 nm for Md_C and Br_C)[3, 11, 15]; M_W is the molecular weight of the FA; ρ_p is the density of FA, equal to 1.79 g/cm^3; φ_p is the effective volume fraction of the adsorbed FA layer and can be expressed by Eq. 12.

$$\varphi_p = 3\frac{Q_{max}r^2}{\rho_p[(l+r)^3-r^3]} \quad (12)$$

Where Q_{max} is the maximum surface concentration, (mg/m^2), which is calculated using the measured BET surface area (135.3 m^2/g for Gt_C, 124.9 m^2/g for Fh_C, 180.2 m^2/g for Md_C and 142.4 m^2/g for Br_C) and the adsorption data of these four colloids presented in previous study[11, 16, 17].

The total modified interaction energy ($V_{T\text{-}Extended}$) could be calculated by Eq. 13.

$$V_{T-Extended} = V_A + V_R + V_{osm} + V_{elas} \quad (13)$$

The UV-absorbance wavelength scanning of the four colloids were shown Fig. S1 (a-d). It was seen that the maximum absorption peaks of Gt_C, Fh_C, Md_C, and Br_C were at 295, 299, 301, and 304 nm, respectively. Hence, the concentration of resulting each colloid suspension was quantified using the ultraviolet (UV) spectrophotometer (UV-1500PC, Macylab Instrument Inc, China) at the wavelength of 300 nm in this study.

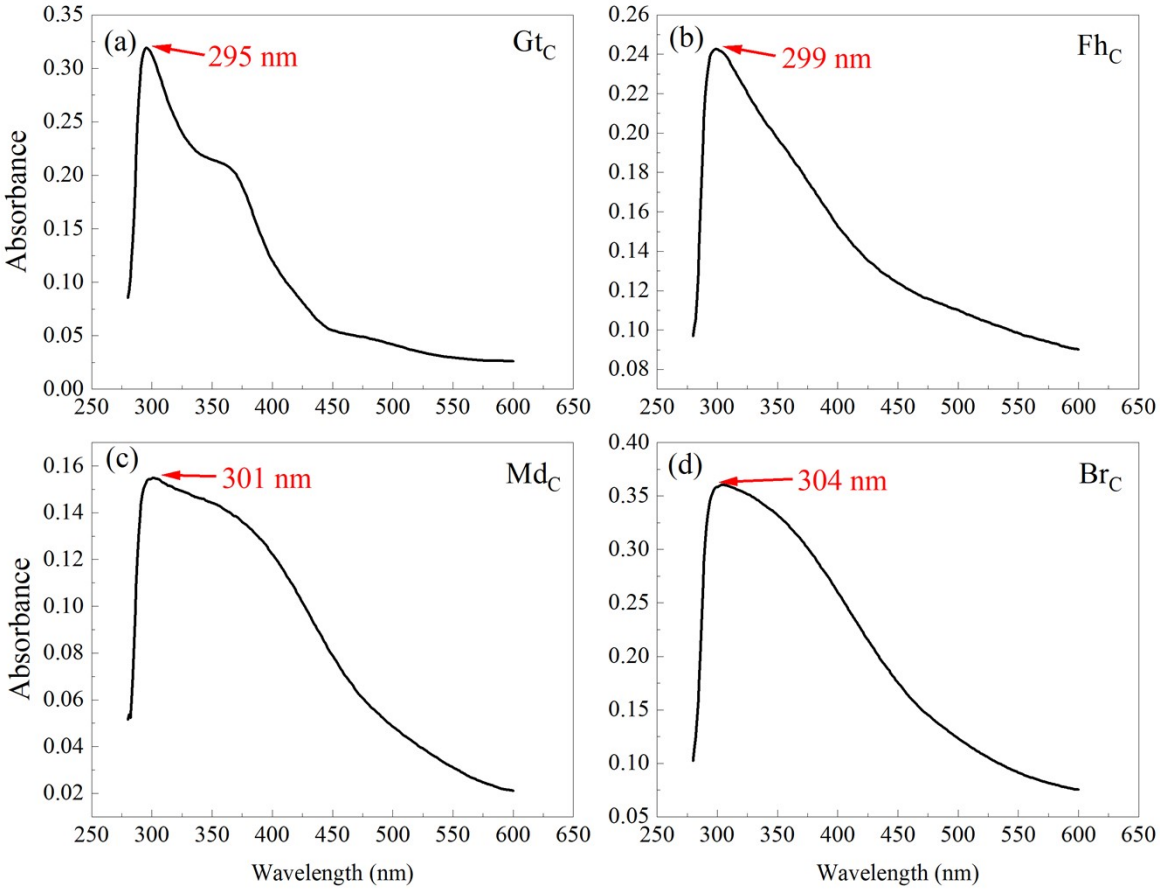

Fig. S1 The UV-absorbance wavelength scanning of 80 mg/L of the four colloids.

The standard curves of the four colloids in concentration of 50-100 mg/L were shown in Fig. S2 (a-d). It was seen that the correlation coefficients (R^2) of Gt_C, Fh_C, Md_C, and Br_C could reach more than 0.995. Hence, the concentration of resulting each colloid suspension was controlled at about 180 mg/L in the colloidal sedimentation experiments in this study.

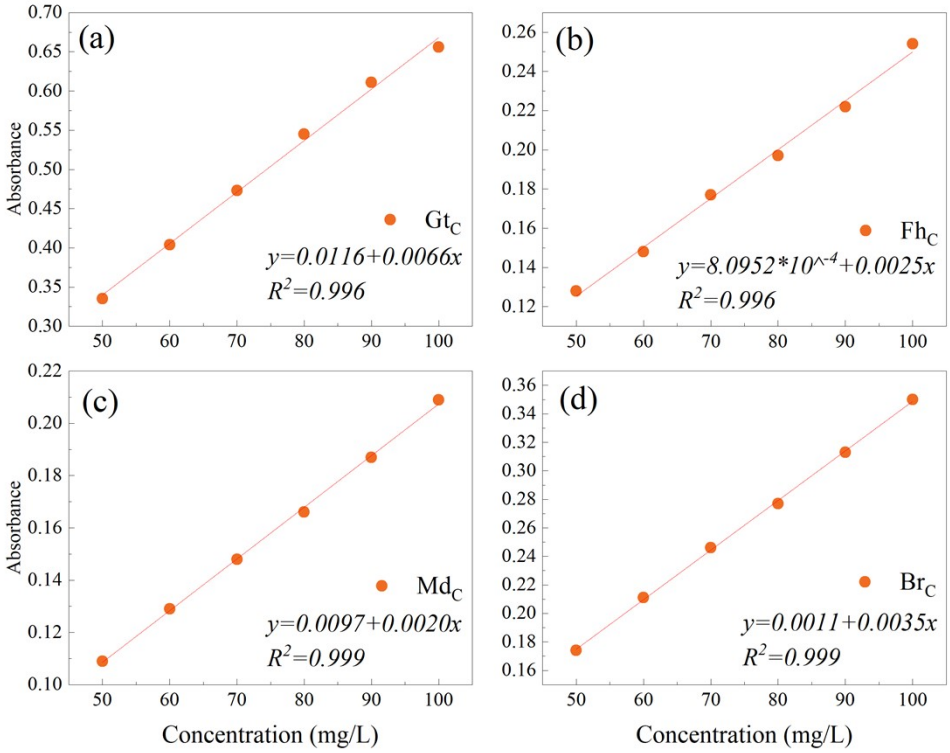

Fig. S2 The standard curves of the four colloids in concentration of 50-100 mg/L.

The X-ray diffraction patterns of goethite, ferrihydrite, pyrolusite, and birnessite were shown in Fig. S3 (a-d). It was seen that diffractions appeared at 2θ values of 17.8°, 21.3°, 26.4°, 33.3°, 34.7°, 36.6°, 40.1°, 41.2°, 53.3°, 59.1°, 61.4°, and 64.0° for goethite; that of 33.4°, and 62.3° for ferrihydrite; that of 37.2°, and 65.1° for pyrolusite; and that of 11.6°, 23.8°, 37.3°, and 67.0° for birnessite, which were consistent with the diffractions of the corresponding standard cards and the current research[2, 5, 18, 19].

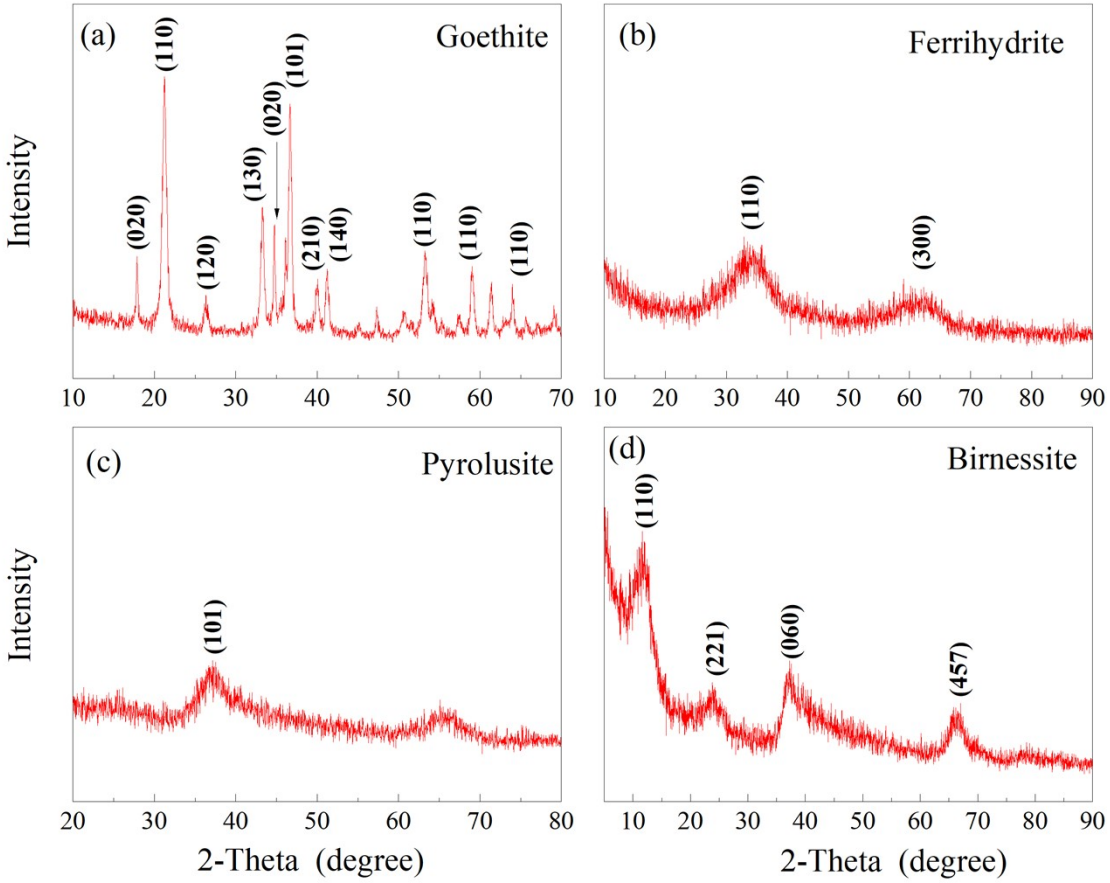

Fig. S3 The X-ray diffraction patterns of (a) goethite, (b) ferrihydrite, (c) pyrolusite, and (d) birnessite.

The surface morphology of Gt_C, Fh_C, Md_C, and Br_C in 1.0 mM-NaCl background solution was shown in Fig. S4. The AFM images also depicted that Gt_C and Fh_C had strip and rounded globular shape, whereas both Md_C and Br_C were irregular aggregates or small colloidal particles.

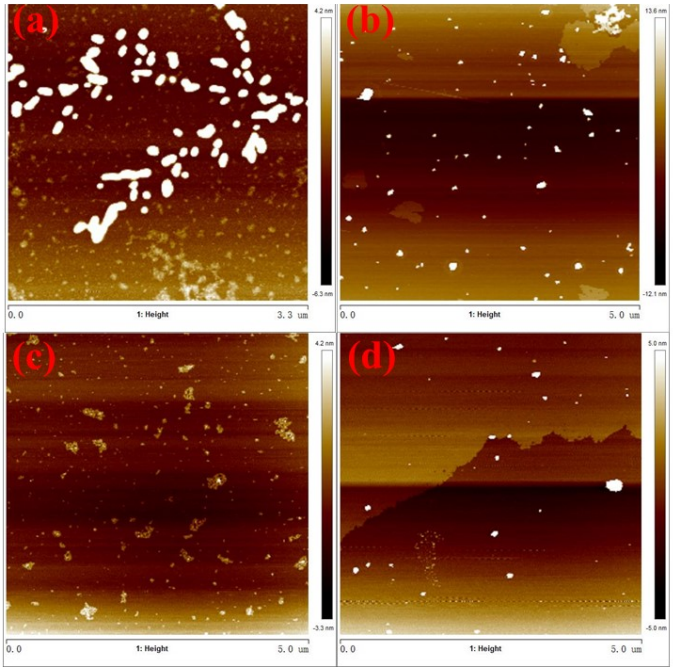

Fig. S4 The surface morphology of Gt_C, Fh_C, Md_C, and Br_C in 1.0 mM-NaCl background solution at pH of 7.0 (colloidal concentration was controlled at 80 mg/L).

The sedimentation kinetics of Gt_C, Fh_C, Py_C, and Br_C at different pH values were shown in Fig. S5 (a-d). It was observed that Gt_C almost settled completely within 24 h at pH of 6.0-8.0, whereas most of Fh_C, Md_C, and Br_C retained.

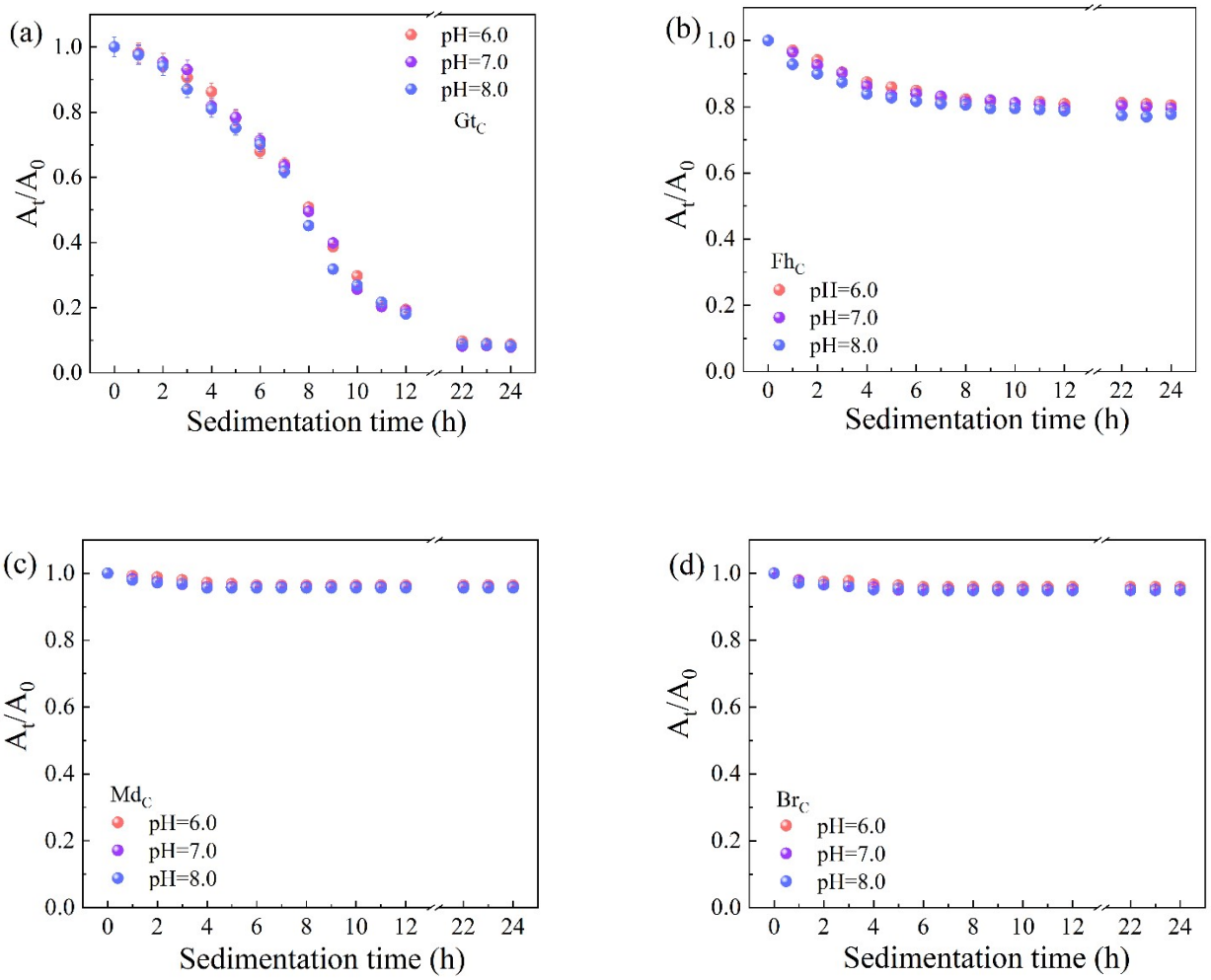

Fig. S5 The sedimentation kinetics of (a) Gt_C, (b) Fh_C, (c) Md_C, and (d) Br_C at different pH values (colloidal concentration was controlled at 80 mg/L).

The sedimentation kinetics of Gt_C, Fh_C, Md_C, and Br_C at different FA concentrations were shown in Fig. S6 (a-d). It was seen that the colloidal retention of Gt_C, Fh_C, Md_C, and Br_C without FA was much less than that with FA. Moreover, the colloidal retention of Gt_C, Fh_C, Md_C, and Br_C increased with the increasing FA concentration.

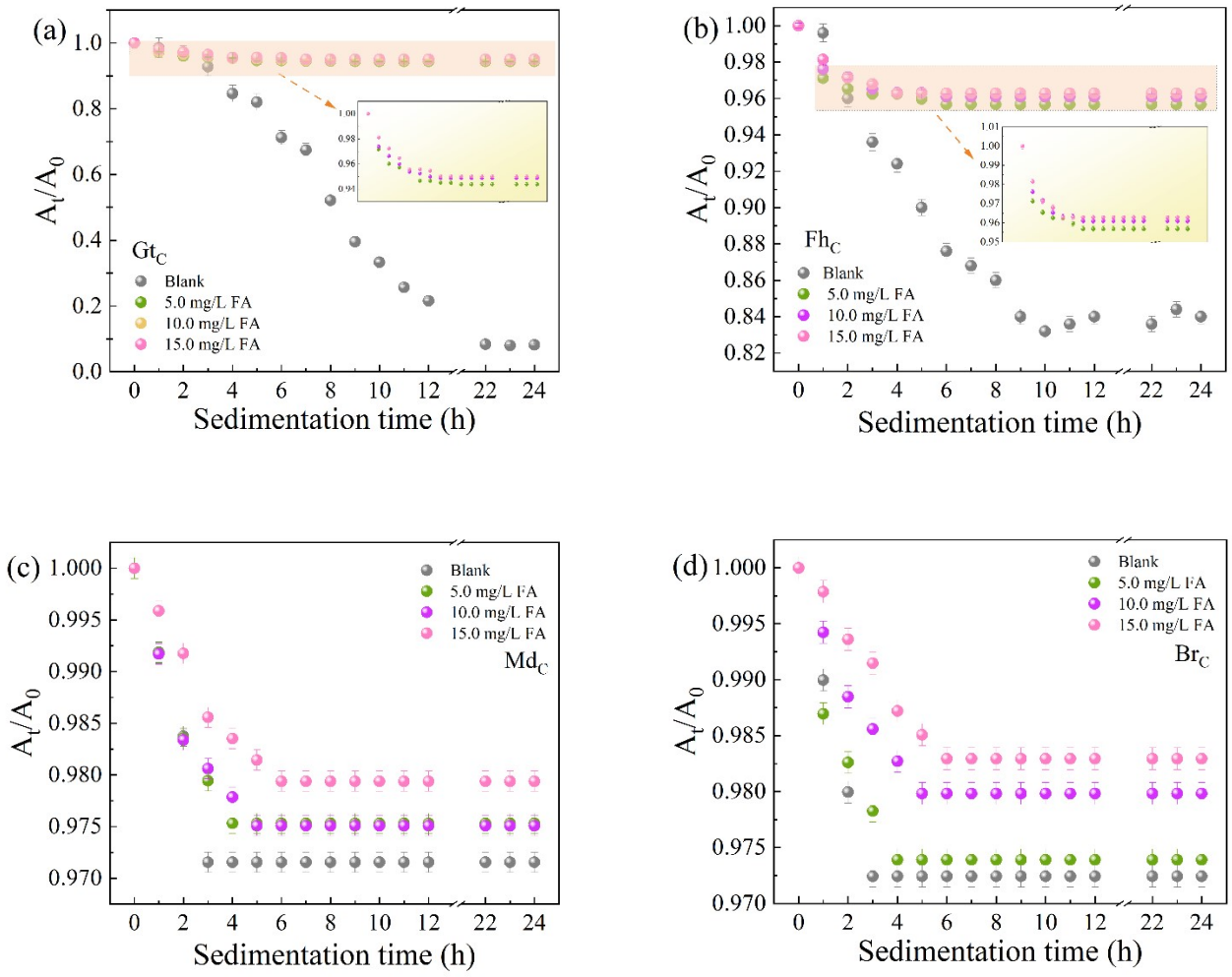

Fig. S6 The sedimentation kinetics of (a) Gt_C, (b) Fh_C, (c) Md_C, and (d) Br_C at different FA concentrations.

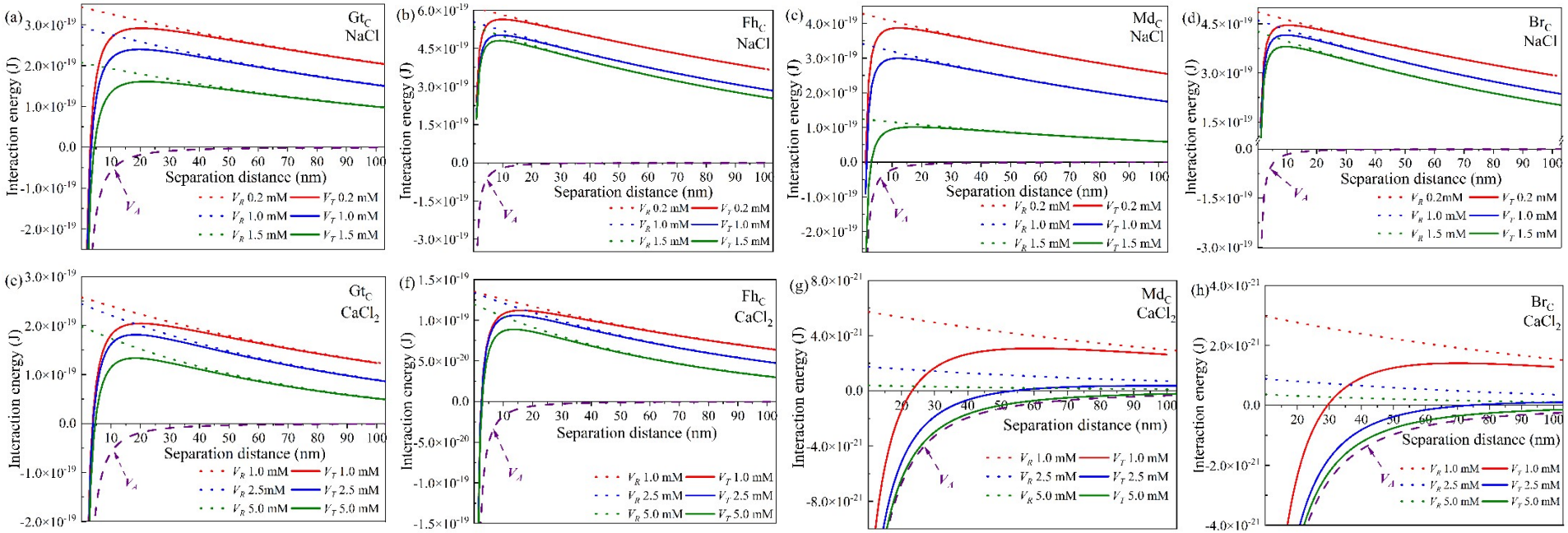

Fig. S7 DLVO interaction energy profiles for Gt_C, Fh_C, Md_C, and Br_C under different concentrations of (a-d) NaCl and (e-h) $CaCl_2$.

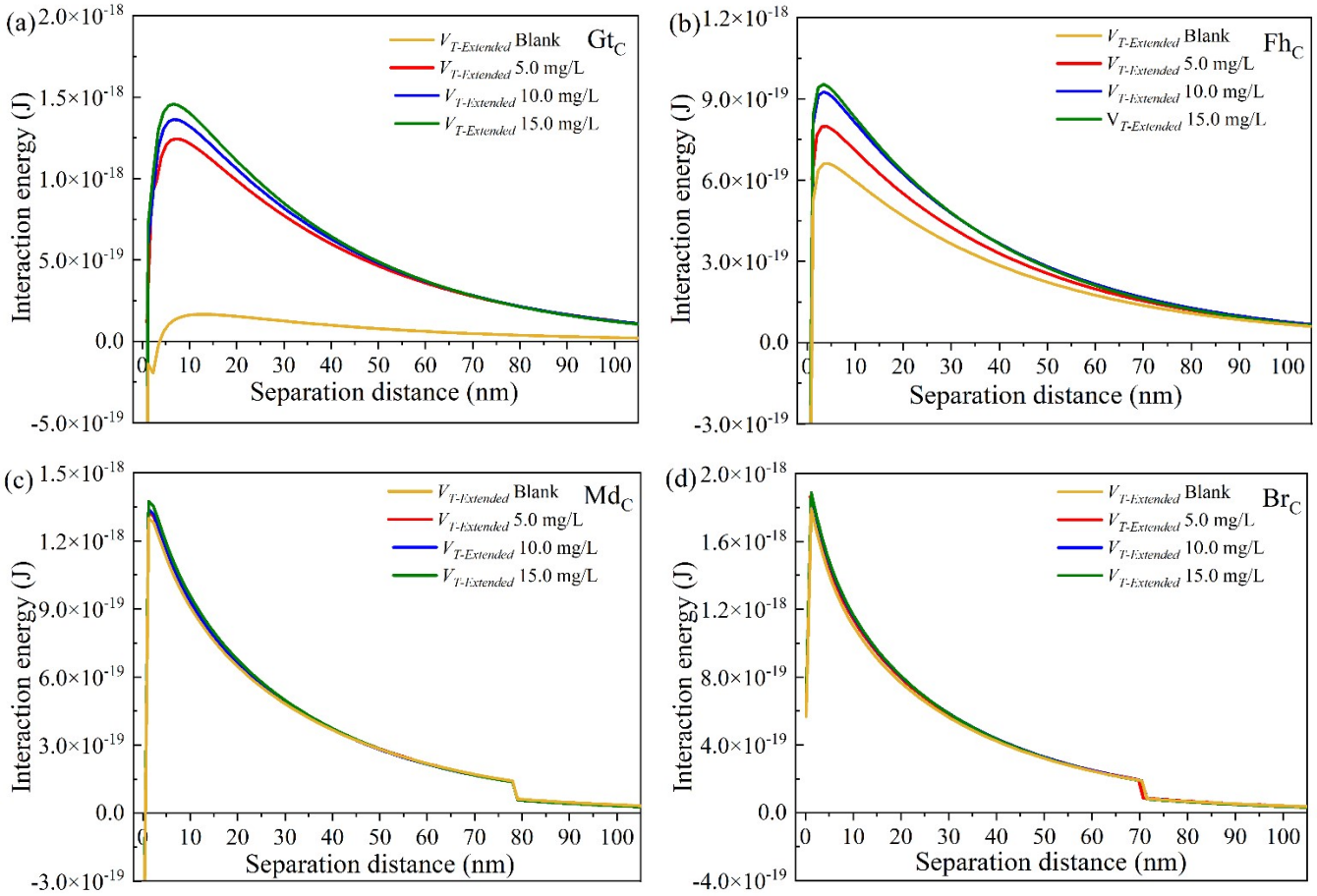

Fig. S8 XDLVO interaction energy curves for Gt_C, Fh_C, Md_C, and Br_C under different concentrations of FA.

Table S1 Predicted sedimentation curves parameters of the four colloids at different electrolyte concentrations.

Test substances	Electrolyte added (mM)	$OD_{plateau}$	OD_1	r_0 (OD/h)	R^2
Gt_C	0.2 Na^+	0.032	1.328	0.061	0.936
	1.0 Na^+	0.015	1.255	0.079	0.926
	1.5 Na^+	0.020	1.239	0.096	0.926
	1.0 Ca^{2+}	0.041	1.113	0.150	0.962
	2.5 Ca^{2+}	0.045	1.097	0.178	0.959
	5.0 Ca^{2+}	0.037	1.117	0.207	0.959
Fh_C	0.2 Na^+	0.830	0.182	0.211	0.984
	1.0 Na^+	0.821	0.189	0.223	0.981
	1.5 Na^+	0.819	0.191	0.245	0.978
	1.0 Ca^{2+}	0.724	0.273	0.101	0.992
	2.5 Ca^{2+}	0.691	0.312	0.093	0.983
	5.0 Ca^{2+}	0.663	0.303	0.108	0.978
Md_C	0.2 Na^+	0.972	0.029	0.506	0.944
	1.0 Na^+	0.971	0.030	0.675	0.983
	1.5 Na^+	0.970	0.031	1.176	1.000
	1.0 Ca^{2+}	0.228	0.760	0.121	0.983
	2.5 Ca^{2+}	0.201	0.768	0.127	0.978
	5.0 Ca^{2+}	0.108	0.824	0.130	0.989
Br_C	0.2 Na^+	0.974	0.027	0.722	0.978
	1.0 Na^+	0.973	0.028	1.240	0.997
	1.5 Na^+	0.971	0.029	2.065	1.000
	1.0 Ca^{2+}	0.596	0.412	0.198	0.986
	2.5 Ca^{2+}	0.507	0.433	0.216	0.973
	5.0 Ca^{2+}	0.349	0.527	0.229	0.967

Table S2 The V_{max} value (J) of the four colloids under different electrolyte and FA concentrations.

Environmental conditions	Gt_C	Fh_C	Md_C	Br_C
0.2 mM Na^+	2.913×10^{-19}	5.641×10^{-19}	3.868×10^{-19}	4.460×10^{-19}
1.0 mM Na^+	2.395×10^{-19}	5.022×10^{-19}	2.997×10^{-19}	4.158×10^{-19}
1.5 mM Na^+	1.608×10^{-19}	4.803×10^{-19}	1.011×10^{-19}	3.804×10^{-19}
1.0 mM Ca^{2+}	2.042×10^{-19}	1.121×10^{-19}	3.071×10^{-21}	1.407×10^{-21}
2.5 mM Ca^{2+}	1.813×10^{-19}	1.059×10^{-19}	3.644×10^{-22}	/
5.0 mM Ca^{2+}	1.334×10^{-19}	8.883×10^{-20}	/	/
without FA	1.655×10^{-19}	6.612×10^{-19}	1.299×10^{-18}	1.793×10^{-18}
5.0 mg/L FA	1.244×10^{-18}	7.985×10^{-19}	1.329×10^{-18}	1.865×10^{-18}
10.0 mg/L FA	1.362×10^{-18}	9.264×10^{19}	1.334×10^{-18}	1.874×10^{-18}
15.0 mg/L FA	1.456×10^{-18}	9.543×10^{-19}	1.374×10^{-18}	1.893×10^{-18}

Reference

1. Paterson, E., Iron oxides in the laboratory. preparation and characterization. *Clay Miner.*, **2000,** *27* (3), 393-393.
2. Wang, D.; Jin, Y.; Jaisi, D.P., Effect of size-selective retention on the cotransport of hydroxyapatite and goethite nanoparticles in saturated porous media. *Environ. Sci. Technol.*, **2015,** *49* (14), 8461-70.
3. Ma, J.; Guo, H.; Lei, M.; Li, Y.; Weng, L.; Chen, Y.; Ma, Y.; Deng, Y.; Feng, X.; Xiu, W., Enhanced transport of ferrihydrite colloid by chain-shaped humic acid colloid in saturated porous media. *Sci. Total Environ.*, **2018,** *621*, 1581-1590.
4. Perez-Benito, J.F.; Arias, C.; Amat, E., A kinetic study of the reduction of colloidal manganese dioxide by oxalic acid. *J. Colloid Interf. Sci.*, **1996,** *177*, 288-297.
5. Tong, F.; Gu, X.; Gu, C.; Xie, J.; Xie, X.; Jiang, B.; Wang, Y.; Ertunc, T.; Schaffer, A.; Ji, R., Stimulation of tetrabromobisphenol a binding to soil humic substances by birnessite and the chemical structure of the bound residues. *Environ. Sci. Technol.*, **2016,** *50* (12), 6257-66.
6. Verwey, E.; Overbeek, J.; Nes, K.V., Theory of the stability of lyophobic colloids : the interaction of sol particles having and electric double l layer. **1948**.
7. Derjaguin, B.V., Theory of stability of highly charged lyophobic sols and adhesion of highly charged particles in solutions of electrolytes. **1941**.
8. Petosa, A. R.; Jaisi, D. P.; Quevedo, I. R.; Elimelech, M.; Tufenkji, N., Aggregation and deposition of engineered nanomaterials in aquatic environments: role of physicochemical interactions. *Environ. Sci. Technol.*, **2010,** *44* (17), 6532-49.
9. Gregory, J., Approximate expressions for retarded van der waals interaction. *J. Colloid Interf. Sci.* **1981,** *83* (1), 138-145.
10. Gregory, J., Interaction of unequal double layers at constant charge. *Journal of Colloid Interface Science* **1975,** *51* (1), 44-51.
11. Huangfu, X.; Jiang, J.; Ma, J.; Liu, Y.; Yang, J., Aggregation kinetics of manganese dioxide colloids in aqueous solution: influence of humic substances and biomacromolecules. *Environ Sci Technol* **2013,** *47* (18), 10285-92.
12. Ma, J.; Jing, Y.; Gao, L.; Chen, J.; Wang, Z.; Weng, L.; Li, H.; Chen, Y.; Li, Y., Hetero-aggregation of goethite and ferrihydrite nanoparticles controlled by goethite nanoparticles with elongated morphology. *Sci Total Environ* **2020,** *748*, 141536.
13. Cheng, H.; Ma, J.; Jiang, J.; Pang, S. Y.; Yang, T.; Wang, P., Aggregation kinetics of manganese oxides formed from permanganate activated by (Bi)sulfite: Dual role of Ca(2+) and Mn(II/III). *Water Res* **2019,** *159*, 454-463.
14. Sun, Y.; Pan, D.; Wei, X.; Xian, D.; Wang, P.; Hou, J.; Xu, Z.; Liu, C.; Wu, W., Insight into the stability and correlated transport of kaolinite colloid: Effect of pH, electrolytes and humic substances. *Environ Pollut* **2020,** *266* (Pt 2), 115189.

15. Wu, A.; Zhao, X.; Yang, C.; Wang, J.; Wang, X.; Liang, W.; Zhou, L.; Teng, M.; Niu, L.; Tang, Z.; Hou, G.; Wu, F., A comparative study on aggregation and sedimentation of natural goethite and artificial Fe(3)O(4) nanoparticles in synthetic and natural waters based on extended Derjaguin-Landau-Verwey-Overbeek (XDLVO) theory and molecular dynamics simulations. *J Hazard Mater* **2022,** *435*, 128876.
16. J.D., F.; D.G., L.; L., M. J. C.; T., H.; V., R. W. H., Adsorption of fulvic acid on goethite. *Geochimica et Cosmochimica Acta,* **2000,** *64(1)*, 51-60.
17. Li, J.; Ding, Y.; Shi, Z., Binding properties of fulvic acid before and after fractionation on ferrihydrite: effects of phosphate. *ACS Earth and Space Chemistry* **2021,** *5* (6), 1535-1543.
18. Wang, X. M.; Yang, K. G.; Sun, S. F.; Xu, J.; Li, Y. G.; liu, F.; Feng, X. H., The structure and composition of ferrihydrite and its environmental geochemical behaviors. *Earth Science Frontiers* **2011,** *18(2)*, 339-347.
19. Jiang, J.; Pang, S. Y.; Ma, J., Oxidation of triclosan by permanganate (Mn(VII)): Importance of ligands and in situ formed manganese oxides. *Environ. Sci. Technol.* **2009,** *43*, 8326-8331.